Far-infrared photon-assisted transport through quantum point-contact devices

Shechao Feng
Department of Physics, University of California, Los Angeles, California 90024

Qing Hu
Department of Electrical Engineering and Computer Science and Research Laboratory of Electronics, Massachusetts Institute of Technology, Cambridge, Massachusetts 02139

(Received 22 February 1993)

We analyze theoretically the phenomenon of photon-assisted quantum transport in split-gate quantum point-contact devices. Both the transverse and longitudinal polarization configurations for the ac photon field are considered. We predict that ministeps should appear in the drain/source conductance versus gate voltage relation, as well as in the I-V_{DS} curve in the nonlinear regime, for a quantum point contact irradiated with a coherent far-infrared radiation. The width of the ministeps is proportional to the radiation frequency and the height of the ministeps is a function of the radiation power. We then calculate the current responsivity for this photon-assisted process in the limit of a small radiation signal and show that it is quite comparable to the quantum efficiency $e/\hbar\omega$ at and above 1 THz if the rf impedance of the device can be matched to that of a planar antenna.

I. INTRODUCTION

Quasiballistic quantum transport through semiconductor quantum point contacts has been an active research area in recent years. In essence, such devices are made of very clean two-dimensional electron gas samples with a finely structured split gate on top of the electron gas, such that the channel width from the source to the drain can be controlled by a negative gate voltage down to a scale of the Fermi wavelength of the electron gas. Thus at low temperatures, electrons can travel from the source to drain without suffering elastic and inelastic scattering. This results in the by now well-known quantized drain/source conductance behavior, with a conductance quantum of $2e^2/h$.[1,2] Extensive work has been done after the discovery of this effect to study the various features and extensions of this quantum transport device.[3] However, most of the experiments that have been performed up to now on such devices are limited to dc transport measurements.

Recently, one of us has proposed a new effect in the quantum point-contact device, namely the *photon-assisted quantum transport*,[4] to study the transport of ballistic electrons under a coherent far-infrared radiation. The frequency of the far-infrared radiation should be in the submillimeter-wave and THz range, which is comparable to that of the intersubband separation at the narrowest constriction. This frequency is too low to excite the normal interband transitions so the two-dimensional electron density remains constant. Only inter- and intrasubband transitions can occur and an electron can absorb energies from the far-infrared photon field to assist its transport over the energy barriers caused by the narrow constrictions of quantum point contacts. Under a finite drain/source bias voltage, a dc photon-induced drain/source current can be produced by the far-infrared radiation. The effect of the photon-assisted quantum transport, if demonstrated experimentally, could be used to develop novel far-infrared devices.

The idea of the photon-assisted quantum transport in a quantum point-contact device is analogous to that of photon-assisted tunneling in superconducting tunnel junctions.[5,6] In a superconducting tunnel junction, quasiparticles (electrons and holes) on one side of the junction can absorb an integer number of photon energy $\hbar\omega$ and raise their energy to tunnel into the other side of the junction. This process can be modeled effectively by using Tien and Gordon's theory of photon-assisted tunneling.[5] In this theory, photon absorption (or emission) is viewed as creating a new set of electron eigenstates, with eigenenergies of $E + n\hbar\omega$, where E is the eigenenergy of the original electron state without radiation. Positive n's correspond to photon absorption and negative n's correspond to photon emission. The probability of absorbing (or emitting) n photons is given by $J_n^2(\alpha)$, where α is a dimensionless number which is proportional to the radiation field strength and inversely proportional to the radiation frequency. The resultant electron density of states is then a superposition of the original density of states with the energy shifted by $n\hbar\omega$ and weighted by the probability factor $J_n^2(\alpha)$. Consequently, the I-V characteristics of an irradiated superconducting tunnel junction is the superposition of the I-V curves of an unirradiated junction with the voltage displaced by $n\hbar\omega/e$, and the current level multiplied by $J_n^2(\alpha)$. These superposed I-V curves form the well-known photon-assisted tunneling steps. In a quantum point contact, similar to the result of the photon-assisted tunneling, the effect of photon absorption on the dc drain/source transport can be viewed as creating a new distribution function of electrons. This new distribution function is a superposition of the original distri-

bution function shifted by $n\hbar\omega$ and weighted by $J_n^2(\alpha)$. Consequently, the curve of the drain/source conductance G_{DS} vs the gate voltage V_{GS} will be a superposition of the original $G_{DS} - V_{GS}$ weighted by $J_n^2(\alpha)$ and shifted by $n\hbar\omega/e\eta$, where η is a dimensionless geometric factor which relates the gate voltage to the energy of the subbands. Thus ministeps should appear on top of well-quantized conductance steps if the photon energy is much higher than the smearing of the conductance steps due to a thermal broadening or a finite drain/source bias voltage.

Motivated by this idea, an experiment on photon-assisted quantum transport in a quantum point contact was performed recently.[7] In this experiment, the split-gate electrodes also serve as the two terminals of a planar log-periodic antenna[8] whose function is to concentrate the radiation field in the central region of the point contact. In this configuration, the polarization of the radiation electrical field is in the transverse direction, thus intersubband transitions can be excited. Preliminary results showed a pronounced drain/source current induced by a coherent radiation at 270 GHz. The photon-induced current is positive right below the gate voltage at which a conductance step occurs and negative above that gate voltage. This is qualitatively what is expected from the photon-assisted quantum transport. The origin of this photon-induced current, however, is unclear because the photon-induced current due to the photon-assisted quantum process will always be accompanied by a current due to heating (or a bolometric effect). These complications are absent in the phenomenon of photon-assisted tunneling in superconducting tunnel junctions,[5,6] in which energy absorption in the leads is prohibited because of the superconducting energy gap.

In order to fully understand the experimental results and, more importantly, to provide guidance for designing future experiments in photon-assisted transport through point contact devices, a more detailed theoretical analysis than the one in the original proposal[4] is needed. In this paper, we provide such a theoretical analysis, based on a combination of WKB approximation and Tien and Gordon's theory of photon-assisted tunneling.[5] We will analyze the photon-assisted transport process due both to intersubband transitions (when the radiation field is in the transverse polarization) and to intrasubband transitions (when the ac field is in the longitudinal polarization). We will demonstrate that, under reasonable approximations, both cases reduce to a one-dimensional problem in which electrons are subject to a dc and an ac potential. In both cases, electrons can raise their energies to above the dc potential barrier by absorbing an integer number of photons. Thus ministeps should be developed on top of the steplike curves for the drain/source conductance vs the gate voltage relation, as well as the nonlinear $I-V_{DS}$ relation for a constant gate voltage. We will point out that the photon-assisted transport process occurs mainly near the classical turning points of a given subband. Thus the key for successfully observing the effect is to concentrate the radiation field into the central region of the point contact device. Finally, we will discuss potential far-infrared applications of the photon-assisted quantum transport by estimating the current responsivity using reasonable device parameters and bias conditions.

There have been several theoretical works on ac transport in quantum point-contact devices recently which we should mention here. In Ref. 9, the effect of an addition of a small ac drain/source voltage on the drain/source conductance is analyzed theoretically. This geometry corresponds roughly to our longitudinal polarized ac radiation case. However, the analysis in this paper was done for a sharp quantum point-contact model, which is somewhat unrealistic for experimentally available samples. Therefore we choose to work with smooth split-gate potentials such that WKB approximation can be used in all regions except near the classical turning points. Also, the theoretical analysis in Ref. 9 was carried out for the one-photon process only. In the far-infrared frequency range, however, multiphoton processes are routine because of the small energy scales of the photons ($\alpha \propto \omega^{-1}$, so that α can be comparable or greater than unity, such that contributions from higher order $J_n's$ can be important). Thus we need to find a theoretical framework to describe general n-photon processes. In Ref. 10, the authors studied theoretically an asymmetric quantum point contact with a transverse polarized ac perturbation. They again restricted their analysis to one-photon processes, but used the realistic smooth potential model. This paper is mainly devoted to the electron-pumping effect at zero drain/source voltage due to an asymmetrical split-gate potential. The nonexponentially small transition rate at high ac frequencies that they find is similar to our conclusions (see Sec. IV). But our main emphasis is on symmetrical split-gate geometry and at a finite drain/source voltage, although it should be very interesting to experimentally study the zero-bias current for the asymmetrical case.

This paper is organized as follows. In Sec. II we shall provide the geometry and theoretical model for our theoretical study. We will discuss the relevant equations of motion separately for longitudinal and transverse polarizations. We will show that for the transverse polarization case, the problem can still be mapped into one which is governed by an effective one-dimensional Schrödinger equation. In Sec. III we calculate approximately the drain/source transmission coefficients and the resulting photoinduced drain/source dc conductance for the longitudinal polarization case, in the presence of an ac perturbation. We will argue that near the classical turning points, the WKB approximation breaks down, which corresponds physically to significant probability for electrons to gain energy from the photon field. In Sec. IV we calculate the transmission coefficients and dc conductance for the transverse polarization. Conclusions similar to the longitudinal case are reached. In Sec. V we will compute the responsivity of the quantum point-contact device under radiation and show that it is within the experimentally interesting range for detector applications. In Sec. VI we discuss the various implications of our results. The key point that energy gaining transitions for transport electrons occur near the classical turning points is stressed. Generalization of our results to the case of

nonlinear $I - V_{DS}$ curves under radiation is made. We also discuss the relevance of our ideas to realistic design of submillimeter wave and THz detectors using quantum point contacts.

II. GEOMETRY AND FORMULATION OF THE MODEL

We consider a standard split-gate quantum point-contact device, as shown in Fig. 1. The electrons are confined to move two dimensionally at the interface of a $GaAs/Al_xGa_{1-x}As$ heterojunction. We assume that the two-dimensional (2D) electron gas has very high mobility such that no impurity potential needs to be included near the constriction region. Two capacitive split gates are patterned on top of the device which forms the constriction for the point-contact device. The shape of the split gates can be described by the distance between them $D(x)$, where the x direction is that of electron transport. The application of a negative gate voltage $-V_G$ creates subband structures in the direction perpendicular to transport (the y direction in Fig. 1). We model the effect of this negative gate voltage on the underneath electron gas by an effective channel width of the electron gas $d(x) \leq D(x)$, which decreases with increasing negative gate voltage. We also assume that the variation of $d(x)$ is slow enough so that WKB-type adiabatic semi-

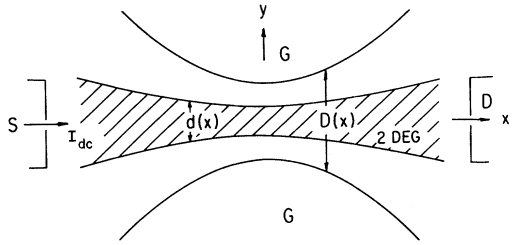

FIG. 1. Geometry of the quantum point-contact device under consideration. We consider the transport properties of a high mobility two-dimensional electron gas (2DEG) which exists at an $Al_xGa_{1-x}As/GaAs$ heterojunction, under an ac photon field. The region G represents the capacitive split gates which are patterned above the 2D electron gas, separated by the $Al_xGa_{1-x}As$ spacer layer with typical thickness of ~ 1000 Å. Upon applying a negative static gate voltage V_G on the two split gates, electrons underneath can be "pushed" out into a region which we represent as the darkened region in this figure. We parametrize the shape of this conducting region by the effective width of the 2D electron gas $d(x)$. The contour of the split gates are parametrized by the spacing between them $D(x) \geq d(x)$. S and D denote the source and drain electrodes, respectively. In the longitudinal polarization, we apply the ac photon field through antenna terminals that are either attached to the S and D electrodes or very close to them, such that the ac electric field is in the x direction, which is the direction of transport. In the transverse polarization configuration, the antenna terminals which couple the ac field into the system are the two split gates themselves, so that the perturbing ac electric field is in the y direction, transverse to the direction of electron transport.

classical approximations for the electron wave function can be applied (with the exception of near the classical turning points; see below). Within this approximation, and assuming infinite potential walls at $y = \pm d(x)/2$, the electron eigenstates can be expressed as products of the longitudinal eigenfunctions $\phi_n(x)$ and the transverse (in the y direction) standing-wave functions $\chi_n(y)$, where

$$\chi_n(y) = \sin\left(\frac{n\pi y}{d(x)}\right), \ n \text{ even},$$

$$\chi_n(y) = \cos\left(\frac{n\pi y}{d(x)}\right), \ n \text{ odd}, \tag{1}$$

with transverse eigenenergies given by

$$E_n(x) = \frac{n^2\pi^2\hbar^2}{2md(x)^2}. \tag{2}$$

This gives rise to the familiar subband structures such that the subband potential energies increase to their maximum values at the narrowest point of the constriction, i.e., $x = 0$ in Fig. 1.

We will in this paper be concerned with two distinct ways in which an ac photon field is applied to the device.

(i) First is longitudinal polarization, where the ac potential for a transporting electron can be written as

$$V_{ac} = -eE_{ac}x\cos(\omega t), \tag{3}$$

where E_{ac} is the ac field strength. This configuration corresponds to the geometry where the antenna terminals which couple the photon radiation into the system are attached on top or near the drain/source electrodes in the point-contact device, as depicted in Fig. 1.

(ii) Second is transverse polarization, where the ac potential is of the form

$$V_{ac} = -eE_{ac}y\cos(\omega t), \tag{4}$$

for $-D/2 < y < D/2$. This physically corresponds to the geometry in which ac radiations are coupled into the sample via the two split gates, i.e., by using the two gates which define the point contact as the two terminals of a planar antenna, such as the device studied in Ref. 7.

We now discuss the basic ingredients of the physical model for the two geometries separately.

A. Longitudinal polarization

In the first case where the ac photon field is polarized in the longitudinal (x) direction, the electron motions in the longitudinal (x) direction and the transverse (y) direction are completely decoupled, such that one can write the longitudinal (x) part of the Schrödinger equation (within the framework of an effective-mass free-electron approximation) governing the electron wave function in the following simple form:

$$\left[-\frac{\hbar^2}{2m}\frac{\partial^2}{\partial x^2} + E_n(x) + V_{ac}(x,t)\right]\phi_n(x,t) = i\hbar\frac{\partial\phi_n(x,t)}{\partial t}. \tag{5}$$

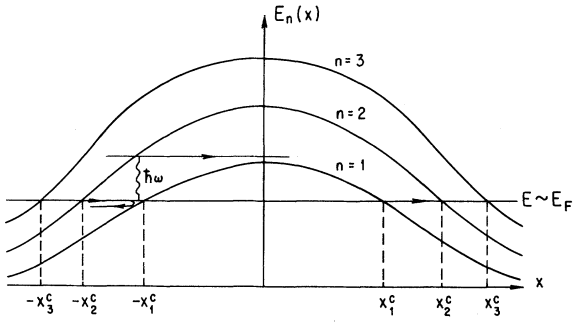

FIG. 2. Effective one-dimensional potential profile for the transport electrons moving from the source to drain in our quantum point-contact device. The barrier potential arises from the various subband energy $E_n(x)$ which is x dependent [cf. Eq. (2)]. Electrons from a particular subband n can propagate adiabatically through the point contact if the electron energy $E \sim E_F$ is larger than the maximum barrier height $E_n(0)$. Under radiation, electrons with energies less than $E_n(0)$ may be able to propagate over the barriers by absorbing an integer number of photons to increase its energy, as illustrated in the figure.

We see here that for the longitudinal configuration, the subband energies due to the split-gate constriction can be viewed as simply a smoothly varying static potential barrier function peaked at $x = 0$. For our consideration of photon-assisted transport through the point-contact device, we are most interested in the regime where $d(0) < \lambda_F/2$ ($\lambda_F = 2\pi/k_F$ where $k_F = \sqrt{2mE_F}/\hbar$ is the Fermi wave vector of the 2D electron gas), such that in the absence of an applied ac photon field the source/drain dc conductance is exponentially small. This is known as the "pinch-off" regime. In this regime any measured dc current is only due to the perturbation of the ac field, such that the device behaves as a sensitive "detector" of the photon field. In this limit the problem is mapped exactly onto a one-dimensional photon-assisted tunneling (or hopping) problem, in which the barrier potential is due to the transverse energy $E_n(x)$ for a given subband, and there is no mixing between the different subbands, at least in the adiabatic limit where we can use WKB-type approximations. We shall see that as a longitudinal ac photon field is applied to the device such that $m\hbar\omega > E_1(0) - E$, transporting electrons of energy E moving in the first subband from source to drain can then "borrow" energy $m\hbar\omega$ by absorbing m photons which allows subsequent adiabatic transmission *above* the barrier, and thus gives rise to a dc photocurrent which are no longer exponentially small. See Fig. 2 for a depiction of this general physical process. We defer our discussion of the solution of this problem to Sec. III.

B. Transverse polarization

In the the second configuration where the ac field is applied in the transverse (y) direction, more care must be taken in separating the Schrödinger equation for the transport electrons from source to drain. In this case, intersubband transitions can occur. Thus, in general, the solutions of the time-dependent Schrödinger equation should include all the subband wave functions, that is,

$$\psi(x,y,t) = \sum_n C_n(x,t)\phi_n(x)\chi_n(y) \tag{6}$$

and

$$\left[-\frac{\hbar^2}{2m}\left(\frac{\partial^2}{\partial x^2}+\frac{\partial^2}{\partial y^2}\right) - eE_{\rm ac}(x)y\cos\omega t\right]\psi(x,y,t) = i\hbar\frac{\partial\psi(x,y,t)}{\partial t}, \tag{7}$$

where $E_{\rm ac}(x) = V_{\rm ac}/D(x)$ is the ac field strength. $\phi_n(x)$ is the longitudinal eigenfunction for the electron in the absence of the ac field, which can be well approximated by the WKB expressions

$$\phi_n(x) \sim \frac{\sqrt{k_n(-L)}}{\sqrt{k_n(x)}}\left[\exp\left(i\int_{-L}^{x}k_n(x')dx'\right) + r_n^0(E)\exp\left(-i\int_{-L}^{x}k_n(x')dx'\right)\right], \quad x \ll -x_n^c$$

$$\phi_n(x) \sim t_n^0(E)\frac{\sqrt{k_n(-L)}}{\sqrt{k_n(x)}}\exp\left(i\int_{x_n^c}^{x}k_n(x')dx'\right), \quad x \gg x_n^c \tag{8}$$

where x_n^c is the classical turning point for subband n, corresponding to the condition $E_n(x_n^c) = E$ (see Fig. 2), and L is the distance from the point contact to the source/drain electrode, which is taken to be larger than all the other length scales in the problem. The x-dependent WKB wave vector

$$k_n(x) = \sqrt{2m[E - E_n(x)]}/\hbar, \tag{9}$$

for electrons moving in the nth subband. $r_n^0(E)$ and $t_n^0(E)$ are the reflection and transmission coefficients at energy E for a given subband n, which determine transport at low temperatures in the absence of an applied ac field.

The corresponding form of the WKB electron eigenfunction $\phi_n(x)$ in the absence of ac field inside the barrier region $-x_n^c \ll x \ll x_n^c$ [for $E < E_n(0)$] is given by a linear combination of tunneling wave functions of the form

$$\phi_n^{\pm} \sim \frac{1}{\sqrt{\kappa_n(x)}}\exp\left(\pm\int_{-x_n^c}^{x}\kappa_n(x')dx'\right),$$

where $\kappa_n(x) = \sqrt{2m[E_n(x) - E]}/\hbar$. The coefficients of the + and − terms are determined by the appropriate

connection formulas [with solutions given in Eq. (8) for the propagating regions $|x| \gg x_n^c$] in the WKB approximation.

It is clear from selection rules that the ac perturbation potential in the transverse polarization geometry mixes the odd and even subbands. As an example of this mixing, we consider the first subband electrons. Multiplying Eq. (7) by $\frac{2}{d}\chi_1(y)$ and then integrating over y from $-d(x)/2$ to $d(x)/2$ leads to

$$i\hbar\phi_1(x)\frac{\partial C_1(x,t)}{\partial t} = \left[-\frac{\hbar^2}{2m}\frac{\partial^2}{\partial x^2} + E_1(x)\right]\phi_1(x,t)C_1(x,t) - eE_{\rm ac}(x)\cos\omega t\sum_{n\geq 2} D_{1n}(x)C_n(x,t)\phi_n(x), \quad (10)$$

where

$$D_{1n}(x) = \frac{2}{d(x)}\int_{-d(x)/2}^{d(x)/2} y\chi_1(y)\chi_n(y)dy.$$

This is the equation of motion for the component of the electron wave function in the first subband, which is coupled via "dipole moments" $D_{1n}(x)$ to those of higher subbands with an odd parity. As the electrons in the first subband has the lowest barrier and thus are the easiest to be excited by the photon field to transmit above the barrier, let us concentrate for the moment on the photon-assisted transmission in this subband. We will generalize our discussion to the case involving higher subband electrons later.

The subband that mixes with the first subband electron the most is the second subband, with a "dipole moment"

$$D_{12}(x) = \frac{2}{d(x)}\int_{-d(x)/2}^{d(x)/2} y\cos[\pi y/d(x)] \times \sin[2\pi y/d(x)]dy = \frac{16d(x)}{9\pi^2} \approx 0.2d(x).$$

The next subband that mixes with the first subband is the fourth subband. As the dipole moment D_{1n} decays quickly with n (for example, $|D_{14}| = \frac{2}{25}D_{12}$), we can then make a further simplification by concentrating on the D_{12} term only. Equation (10) then reduces to the form

$$\left[-\frac{\hbar^2}{2m}\frac{\partial^2}{\partial x^2} + E_1(x) + V_1^{\rm eff}(x,t)\right]\psi_1(x,t) = i\hbar\frac{\partial\psi_1(x,t)}{\partial t}, \quad (11)$$

where we have rewritten $\psi_1(x,t) \equiv \phi_1(x)C_1(x,t)$, and have introduced an effective time-dependent perturbation potential

$$V_1^{\rm eff} = -eD_{12}(x)E_{\rm ac}(x)\cos(\omega t)\frac{\phi_2(x)}{\phi_1(x)}\frac{C_2(x,t)}{C_1(x,t)} \approx -0.2eV_{\rm ac}\frac{d(x)}{D(x)}\frac{\phi_2(x)}{\phi_1(x)}, \quad (12)$$

where we have approximated the two C functions to be the same, which is certainly valid in regions $|x| \gg x_1^c, x_2^c$, where the two subband energies $E_1(x)$ and $E_2(x)$ are essentially the same and both are small. We will now see that even when x is close to the origin, the effective ac perturbation potential is still dominated by the ratio of the two ϕ functions.

In particular, since the $\phi_2(x)$ function changes from being propagating (from $x = -\infty$) to an essentially exponentially decaying function when $x > -x_2^c$, while the $\phi_1(x)$ function remains propagating until $x \approx -x_1^c > -x_2^c$ (see Fig. 2), we observe that $V_1^{\rm eff}$ will drop to zero very quickly near $x \geq -x_2^c$. As we shall see, it is this sharp change in the effective ac perturbation potential near x_n^c that produces substantial transition by an electron to gain energy from E (close to E_F) to $E + m\hbar\omega$ so as to transmit above the barrier $[E_1(x)]$ without suffering the usual exponentially small tunneling probability due to the barrier potential.

Thus we see that with suitable approximations, we can still map the photon-assisted electron transport problem in the case of transverse polarization into an effective one-dimensional Schrödinger equation with a sinusoidal ac perturbation potential, in essentially the same form as in the longitudinal polarization case.

So for both cases, our problem is now reduced to one of solving for the effective transmission coefficients for an electron to propagate from the left reservoir (the source), at starting energy E and subband n, to the right reservoir (the drain), subjecting to a static potential barrier $E_n(x)$, upon absorbing m photons (and thus raising its energy to $E + m\hbar\omega$), which we denote as $T_n(E, m\hbar\omega)$. Once we have obtained these transmission coefficients, the dc source/drain (linear) conductance can be then written, using the Landauer formula,[11]

$$G = 2\frac{e^2}{h}\sum_{n=1}^{\infty}\int_{-\infty}^{\infty} dE\left(-\frac{\partial f}{\partial E}\right)g_n(E)v_{nx}(E)\sum_{m=-\infty}^{\infty}T_n(E, m\hbar\omega) = 2\frac{e^2}{h}\sum_{n=1}^{\infty}\int_{-\infty}^{\infty} dE\left(-\frac{\partial f}{\partial E}\right)\sum_{m=-\infty}^{\infty}T_n(E, m\hbar\omega), \quad (13)$$

since the density of states for a given subband electron $g_n(E)$ is given by $g_n(E) = 1/v_{nx}(E)$.

In the absence of an ac photon field, we have for smooth split-gate potentials the well known WKB result

$$T_n(E) = \theta[E - E_n(0)],$$

up to exponentially small factors in $\exp[-k_n(0)R]$, where R is the radius of curvature of the $d(x)$ function at $x = 0$, and $k_n(0)$ is given in Eq. (9).[12] This gives at low temperatures for the dc conductance

$$G = 2\frac{e^2}{h}\sum_{n=1}^{\infty} f_T\{-[E_F - E_n(0)]\}.$$

In the limit $T \to 0$ we recover the simple result

$$G = 2\frac{e^2}{h}N,$$

where N is the index of the highest subband which obeys $E_F > E_n(0)$, i.e., which allows adiabatic transmission through the point contact. This gives rise to the step-like quantized conductance structure for quantum point-contact devices.[1,3]

III. CALCULATING THE LINEAR dc PHOTOCURRENT IN THE LONGITUDINAL POLARIZATION

We now present approximate calculations of the photoinduced electron transmission coefficients $T_n(E, m\hbar\omega)$, in the configuration where the ac field is applied along the same direction as the dc bias, i.e., in the x direction, and then compute the linear dc conductance using the Landauer formula given above.

From Eq. (5) and the form of the WKB eigenfunctions in the absence of an ac perturbation in Eq. (8), we may derive the perturbed WKB wave functions by looking at the next-order corrections in the phase function, defined by (suppressing for the moment the subband index n)

$$\phi(x,t) \approx \frac{\sqrt{k_n(-L)}}{\sqrt{k_n(x)}}\exp[iS(x,t)/\hbar], \tag{14}$$

with

$$S(x,t) = S_0(x,t) + S_1(x,t) + \cdots.$$

The zero-order solution, in the propagating regions $x < -x_n^c$ (for subband n), is of course the standard WKB expression

$$S_0(x,t) = -Et + \int_{-L}^{x} k(x')dx',$$

where $k(x) = \sqrt{2m[E - E_n(x)]}/\hbar$.

The next-order correction to the phase function in the same region $x < -x_n^c$ in the presence of the ac perturbation potential $V_{\rm ac}(x)$ obeys the differential equation (set $\hbar \equiv 1$)

$$\frac{\partial S_1(x,t)}{\partial t} = -\frac{k(x)}{m}\frac{\partial S_1(x,t)}{\partial x} - eV_{\rm ac}(x)\cos(\omega t). \tag{15}$$

This equation can be integrated exactly to yield

$$S_1(x,t) = \tilde{S}_1(x,\omega)\exp(i\omega t) + \tilde{S}_1(x,-\omega)\exp(-i\omega t),$$

where the function $\tilde{S}_1(x,\omega)$ is given by

$$\tilde{S}_1(x,\omega) = -\frac{m}{2}\exp[-i\omega\tau(x)] \times \int_{-L}^{x} dx' \frac{\exp[i\omega\tau(x')]}{k(x')}V_{\rm ac}(x'). \tag{16}$$

The "time" function $\tau(x)$ is defined as

$$\tau(x) = \int_{-L}^{x} dx' \frac{m}{k(x')},$$

which is a kind of semiclassical time for a wave packet to travel from the source (at $x \to -L$) to the point x.

After some manipulations, we can rewrite for the perturbed incident wave function ($x < -x_n^c$)

$$\phi(x,t) \approx \frac{\sqrt{k(-L)}}{\sqrt{k(x)}}\sum_{k=-\infty}^{\infty} J_k[2|\tilde{S}_1(x,\omega|)]\exp\left[i\int_{-\infty}^{x} k(x')dx' + ik[\beta(x,\omega) + \pi/2]\right]\exp[-i(E + k\omega)t], \tag{17}$$

where $\beta(x,\omega)$ is the phase factor of the complex function $\tilde{S}_1(x,\omega)$ and $J_k(x)$ is the kth-order Bessel function.

Inside the barrier region $|x| \ll x_n^c$, one can similarly write down the WKB perturbed wave function in the form

$$\phi(x,t) \approx A\sum_{k=-\infty}^{\infty} J_k[2|\tilde{S}_1(x,\omega|)] \times \exp\left[-i(E + k\omega)t - \int_{-x_n^c}^{x}\kappa(x')dx' + ik[\beta(x,\omega) + \pi/2]\right], \tag{18}$$

where $\kappa = \sqrt{2m[E_n(x) - E]}/\hbar$, $\beta(x,\omega)$ is the phase factor of the complex function

$$\tilde{S}_1(x,\omega) = i\frac{m}{2}\exp[+\omega\tilde{\tau}(x)] \times \int_{-x_n^c}^{x} dx' \frac{\exp[-\omega\tilde{\tau}(x')]}{\kappa(x')}V_{\rm ac}(x'),$$

with $\tilde{\tau}(x) = \int_{-x_n^c}^{x} dx' \frac{m}{\kappa(x')}$ being a kind of "imaginary" time. The value of $\tilde{\tau}(x_n^c)$ symbolizes the characteristic time for the tunneling electron to spend under the barrier in the WKB approximation.[13,14] The coefficient A

must be found by connecting the wave function under the barrier to the incident and the reflected wave function in the $x < -x_n^c$ region using the WKB connection formulas.

Very similar expressions to that in Eq. (17) can be written down for the perturbed WKB wave functions in the region $x > x_n^c$, which seems to mean that one can now derive, within the WKB approximation, the perturbed transmission coefficients $T_n(E, m\hbar\omega)$.

But as we can observe from Eq. (18), the WKB wave function in the barrier region is still dominated by the exponentially decaying (zeroth-order) term $\sim \exp[-\int_{-x_n^c}^{x} \kappa(x')dx']$, even in the presence of the ac perturbation. Thus WKB approximation will not yield the above-barrier transmission [at $m\hbar\omega > E_n(0) - E$] that we anticipate from intuitive considerations.

The reason for this apparent failure of the WKB approach is that near the classical turning point $x \approx -x_n^c$, the WKB approximation *breaks down*, as both $k(x)$ and $\kappa(x)$ approach zero, and the various correction terms (within WKB) $S_1(x,t)$ diverge. This physically corresponds to real transitions such that electron gains energy $m\hbar\omega$ from the photon field, so that its new energy $E + m\hbar\omega$ is above the barrier height.

In order to understand the nature of these energy absorbing transitions near $x = -x_n^c$, let us consider a linearized form of the barrier potential

$$E_n(x) - E \approx F(x + x_n^c),$$

with F being a local "force" at the classical turning point. The wave function in the absence of ac perturbations can be written in the Fourier (k) space as ($\hbar \equiv 1$) (Ref. 15)

$$\tilde{\phi}_0(k) \sim \exp\left[-\frac{i}{F}(Ek - k^3/6m)\right].$$

In the presence of the ac perturbation, we can write the Schrödinger equation in k space as

$$i\frac{\partial\tilde{\phi}(k,t)}{\partial t} = \left(-\frac{k^2}{2m} + F\frac{\partial}{i\partial k} + eE_{\rm ac}\cos(\omega t)\frac{\partial}{i\partial k}\right)\tilde{\phi}(k,t). \tag{19}$$

Using the ansatz

$$\tilde{\phi}(k,t) = \sum_n \tilde{\phi}_n(k)\exp[-i(E + n\omega)t],$$

one can show that the perturbed wave function is given by

$$\tilde{\phi}(k,t) = \sum_n J_n\left(\frac{eE_{\rm ac}}{\hbar\omega}\frac{\partial}{i\partial k}\right)\tilde{\phi}_0(k)\exp[-i(E + n\omega)t]. \tag{20}$$

As an example, we consider the one-photon process $n = 1$, in the limit of a small ac field such that we may use the approximation $J_1(x) \approx x$ for small x. This gives for the first-order correction to the wave function

$$\tilde{\phi}_1(k,t) \approx \frac{eE_{\rm ac}l_1(E,k)}{\omega}\tilde{\phi}_0(k)\exp[-i(E + \omega)t], \tag{21}$$

with $l_1(E,k) \equiv -\frac{E}{F} + \frac{k^2}{2Fm}$ being a length scale whose physical meaning will become clear later. Suppose that the new energy $E + \omega$ is higher than the barrier height $E_n(0)$; then the amplitude transmission coefficient can be obtained by taking the overlap integral between this one-photon-assisted wave function $\tilde{\phi}_1(k,t)$ and the zeroth-order WKB wave function $\phi^0_{E+\omega}$ at $E + \omega$ with wave vector $k_1(x) = \sqrt{2m[E + \omega - E_n(x)]}/\hbar$ (which is a real quantity throughout the system):

$$\phi^0_{E+\omega} \sim \frac{1}{k_1(x)}\exp\left(i\int^x k_1(x')dx'\right),$$

yielding a result (with the understanding that electron at the new state $E + \omega$ and k_1 can propagate above the barrier adiabatically with negligible reflection)

$$t(E,\omega) \approx \frac{eE_{\rm ac}l_1(E,\omega)}{\omega}, \tag{22}$$

with $l_1(E,\omega) = \frac{E+\omega}{2F}$. It is important to note that there is no exponentially small factor in this expression for the amplitude transmission coefficient, since electrons in an initial state $E < E_n(0)$ have made a real transition to a final state $E + \omega > E_n(0)$ by absorbing a photon from the ac perturbations so as to be able to transmit across the quantum point contact above the barrier potential.

Thus, in the following, we shall use a simplified approximate model to describe the photoinduced over-the-barrier transmission in quantum point-contact devices with a longitudinal polarization: an incoming electron propagates with $k(x) = \sqrt{2m[E - E_n(x)]}/\hbar$ in the region $x < -x_n^c$, and then propagates in the region $x > -x_n^c$ with $k_m = \sqrt{2m[E + m\omega - E_n(x)]}/\hbar$ associated with an m-photon absorption process. The energy of the electron will be increased to $E + m\omega$. The probability amplitude for absorbing m photons will be assumed to be $J_m^2(\alpha_m)$, with $\alpha_m \approx eE_{\rm ac}l_m(E,k_m)/\hbar\omega$, with $l_m(E,k_m)$ being a length scale determined from the detailed analysis of the mth term in Eq. (20). As we have seen in the one-photon example, $l_1(E,k_m) = -\frac{E}{F} + \frac{k_m^2}{2Fm}$, where $F = \frac{dE_n(x)}{dx}|_{-x_n^c}$ [cf. Eq. (21)]. Typically, we can estimate $l_m(E,k_m) \approx x_n^c$, as long as the incoming energy is not too close to the top of the barrier function $E_n(0)$. For those values of m such that $E + m\omega$ is larger than the barrier height $E_n(0)$, the induced electron wave function can transmit across the barrier without suffering the exponentially forbidding factor for elastic tunneling at $E < E_n(0)$. We will estimate the corresponding m-photon absorbing transmission coefficient by assuming the existence of a *sharp* potential step at $x = -x_n^c$, due to the sudden change of the wave vector from k to k_m. The mismatch at $x = -x_n^c$ will be modeled simply by requiring that the wave functions themselves as well as their first derivatives in the two regions be continuous at $x = -x_n^c$. Again, we emphasize that this rather drastic simplification is approximately justified because near $x = -x_n^c$, the parameter which relates the ratio of successive WKB correction terms, namely $\frac{1}{kE_n(x)}\frac{eE_n(x)}{dx}$, diverges as k (or κ) $\to 0$, leading to a complete breakdown of the WKB approximation which tends to keep

the electron from making sizable transitions to a state with larger wave vector. Within this approximation, we can now estimate for the transmission probability

$$T_n(E, m\omega) \approx \theta[E + m\omega - E_n(0)] \left(\frac{2k_n}{k_n + k_n^m}\right)^2 J_m^2(\alpha_n^m), \tag{23}$$

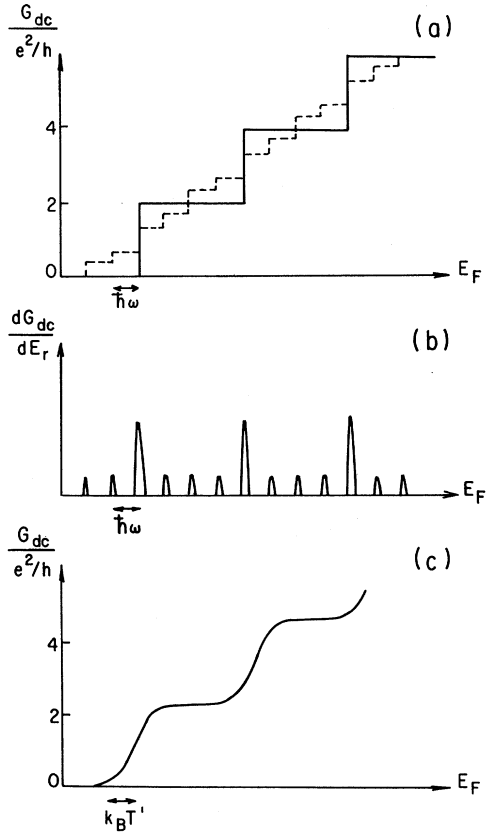

FIG. 3. (a) The predicted drain/source dc conductance (or current) as a function of changing Fermi energy E_F, at low temperatures such that $\hbar\omega \gg k_BT$, and at a very low source/drain bias voltage. In real experiments, the horizontal axis could be the gate voltage V_G relative to that corresponding to the total pinch-off case. The solid line denotes the conductance plateau behavior in the absence of an ac photon field. The dotted line indicated the changes to the dc current as a result of photoinduced transport, resulting from Eq. (24). The distance from each steplike decoration to the original quantized conductance step position is given by $m\hbar\omega$ ($m = \pm1, \pm2, \ldots$), and the height of these ministeps is roughly the sum of $J_m^2(\alpha)$ (see text). (b) The derivative of I_{dc} with respect to the Fermi energy (or gate voltage). Minipeaks due to photoinduced dc current appear on each side of an original quantized conductance step. The width of the minipeaks is $\sim k_BT$, and the minipeaks are separated from each other by the photon energy $\hbar\omega$. (c) I_{dc} vs E_F due to simple temperature broadening $T \to T' > T$. Essentially the same behavior can be expected for the differential conductance $g = dI_{dc}/dV$ as a function of the dc bias voltage in the nonlinear regime, for a fixed gate voltage which is biased in the pinch-off limit.

where we have put the subband index back into our expressions, and $\alpha_n^m \approx eE_{ac}l_{n,m}(E, k_m)/\hbar\omega$. As a further simplification, we can take for the original $k_n \approx \sqrt{2mE}/\hbar$ (i.e. for x far from the classical turning point on the left) and $k_n^m \approx \sqrt{2m[E + m\omega - E_n(0)]}/\hbar$ at the middle of the barrier region. The θ function indicates the fact that nonexponentially small transmission through the barrier is possible only when the electron has acquired enough energy from the photon field to be propagating above the barrier potential.

Using this estimated result for the transmission coefficient for the m-photon absorption process, together with the Landauer formula Eq. (13), we can now write down the estimated linear photoinduced dc current as

$$I_{dc} \approx \Delta V_{dc} \frac{2e^2}{h} \sum_{n=1}^{\infty} \sum_{m=-\infty}^{+\infty} f_T\{-[E_F + m\hbar\omega - E_n(0)]\} \times J_m^2(\alpha_n^m) \left(\frac{2k_n}{k_n + k_n^m}\right)^2, \tag{24}$$

where ΔV_{dc} is the source/drain dc voltage, and we use the following estimate for α_n^m: $\alpha_n^m \approx eE_{ac}x_n^c/\hbar\omega$.

We plot on Fig. 3 the expected behavior of I_{dc} implied by Eq. (24) when the Fermi energy is varied, at low values of ΔV_{dc} and at low temperatures such that $k_BT \ll \hbar\omega$, such that the Fermi function $f_T(E)$ can be well approximated by $\theta(-E)$, for a value of $\alpha_n^m \approx 1$. In this limit we expect the appearance of "mini"-steps near the original conductance steps, separated by $\hbar\omega$ in energy, and with magnitudes given by the sum of $J_n^2(\alpha_n^m)(\frac{2k_n}{k_n+k_n^m})^2$. In real experimental situations, E_F is usually fixed, and one changes the (negative) gate voltage V_G so that the 2D electron gas width $d(x)$ is changed, whereby varying $E_n(0)$. Thus the horizontal axis can be thought of as $|V_G^{max}| - |V_G|$, where V_G^{max} is the value of the gate voltage corresponding to the "pinch"-off limit of the device, i.e., when $d(x) \to 0$. If we take a derivative of the I_{dc} dependence on the Fermi energy (or gate voltage), we then expect to observe a series of "satellite" peaks around each conductance peak, of width $\sim k_BT \ll \hbar\omega$, and with an integrated area given by the sum of $J_n^2(\alpha_n^m)(\frac{2k_n}{k_n+k_n^m})^2$. This is depicted in Fig. 3(b).

IV. dc PHOTOCURRENT IN THE TRANSVERSE POLARIZATION

In this section we calculate the corresponding photoinduced dc linear current in the transverse polarization, i.e., when the ac photon field is coupled to the electron gas through the split gates as antennas.

From Eq. (11), we see that the transverse polarization case can be approximately treated (at least for the first subband electrons) as a one-dimensional Schrödinger problem in the presence of a periodic ac perturbation potential, $V_1^{eff}(x)\cos(\omega t)$ for the first subband electrons, with the corresponding transmission coefficients. Thus our calculation can proceed accordingly.

There is an important difference between the trans-

verse and the longitudinal polarization cases though. In the longitudinal case, the ac potential is smooth throughout the device, but the effective wave vector $k(x)$ or $\kappa(x)$ go to zero near the classical turning point, thus enhancing the transition processes for the transport electron to gain photon energy so as to transmit above the barrier. In the transverse polarization case, the effective ac potential for the first subband electrons [the dominant ones for $E_F \leq E_1(0)$], given in Eq. (12), goes to zero rapidly near $-x_2^c$, the classical turning point of the *second* subband, which is left to the corresponding classical turning point $-x_1^c$ for the first subband. At this position $x \sim -x_2^c$, the WKB electron wave vector $k_1(x)$ is still quite smooth and real, while the ac perturbation potential $V_{\rm ac}^{\rm eff}(x)$ goes to zero rapidly. The rate of change of $V_{\rm ac}^{\rm eff}(x)$ near $-x_2^c$ is approximately $\kappa_2(\lambda_1)$, where $\lambda_1 = 1/k_1(x_2^c) \approx d(x_2^c)$. Thus the parameter which sets the ratio between successive terms in the WKB approximation,

$$\frac{dV_1^{\rm eff}(x)}{dx}\frac{\lambda_1}{V_1^{\rm eff}(x)},$$

is of order unity. This indicates that there will be significant transitions of the transporting electron to gain energy from the photon field, induced by the rapid variations of the $V_1^{\rm eff}(x)$ perturbation potential at $x \geq -x_2^c$, similar to the situation in the longitudinal case. Whereas near the classical turning point $-x_1^c$, as the perturbing potential $V_1^{\rm eff}(x)$ is already very small, no significant transitions will occur.

We will describe the energy gaining transitions by the transporting electrons near $-x_2^c$ using the same approximations as in the longitudinal polarization case, namely, by assuming that there is an effective sharp boundary at $x = -x_2^c$, with the electron wave function at $x < -x_2^c$ being of the form

$$\psi(x,t) \sim \sum_m J_m(\alpha)\left(\exp\left[i\int^x k_1(x')dx'\right] + r\exp\left[-i\int^x k_1(x')dx\right]\right) \times \exp[-i(E+m\omega)t], \quad (25)$$

with $k_1(x) = \sqrt{2m[E - E_1(x)]}$, and the wave function at $x > -x_1^c$ having the form

$$\psi(x,t) \sim \sum_{m>m_c} A_m \exp\left[i\int^x k_1^m(x')dx' - i(E+m\omega)t\right], \quad (26)$$

where $k_1^m = \sqrt{2m[E+m\omega - E_1(x)]}$ (for the first subband electrons) and $\alpha \approx eV_1^{\rm eff}(-x_2^c)/\hbar\omega$. The sum in the above wave function only includes terms such that $E + m\hbar\omega > E_1(0)$, so that electrons can propagate above the barrier, upon absorbing energy from the photon field. By matching the boundary conditions at $x = -x_2^c$, we again find for the transmission coefficients for the nth subband electrons which transmit above the barrier after absorbing m photons given approximately by

$$T_n(E, m\omega) \approx \theta[E + m\omega - E_n(0)]\left(\frac{2k_n}{k_n + k_n^m}\right)^2 J_m^2(\alpha_n), \quad (27)$$

where $k_n = \sqrt{2m[E - E_n(x_{n+1}^c)]}/\hbar$ and $k_n^m = \sqrt{2m[E + m\hbar\omega - E_n(x_{n+1}^c)]}/\hbar$, and $\alpha_n \approx eV_{\rm ac}^{\rm eff}(x_{n+1}^c)/\hbar\omega$.

The corresponding dc current expression can also be obtained analogously:

$$I_{\rm dc} \approx \Delta V_{\rm dc}\frac{2e^2}{h}\sum_{n=1}^{\infty}\sum_{m=-\infty}^{+\infty} f_T\{-[E_F + m\hbar\omega - E_n(0)]\} \times J_m^2(\alpha_n)\left(\frac{2k_n}{k_n + k_n^m}\right)^2. \quad (28)$$

Thus qualitatively, we expect the same behavior in photon-assisted transport in a quantum point contact, in both the transverse and the longitudinal polarizations.

V. ac DISSIPATION POWER AND CURRENT RESPONSIVITY

The current responsivity of a detector is defined as

$$R_I = \frac{\Delta I_{\rm dc}}{P_{\rm ac}},$$

where $\Delta I_{\rm dc}$ is the photon-induced drain/source current which is defined as the difference between the drain/source current with and without radiation, and $P_{\rm ac}$ is the power dissipation at the ac frequency. In our device, this quantity is fairly easy to estimate. In both the longitudinal and the transverse polarizations, the main power dissipation of the ac field is in the large 2D electron gas region. At a few λ_F away from the center of the quantum point contact, the free-carrier ac conductance can be modeled using the Drude model:

$$G_{\rm ac} = \frac{G_\square}{1 + (\omega\tau)^2}, \quad (29)$$

where $G_\square$ is the dc sheet conductance of the 2D electron gas, which for a typical modulation-doped field-effect transistors (MODFET) structure is on the order of 0.1 Ω^{-1} at temperatures lower than 10 K. The relaxation time (corresponding to the total relaxation rate) τ is related to the electron mobility through

$$\tau = \frac{\mu m}{e}.$$

For high-quality GaAs/Al_xGa_{1-x}As MODFET devices, $\mu \approx 10^6$ cm^2/V s, which gives $\tau \approx 40$ ps. Thus $\omega\tau \gg 1$ in the submillimeter-wave frequency range $f \geq 300$ GHz in our consideration. The ac power dissipation from the 2D electron gas (i.e., away from the point-contact center) is then given by

$$P_{\rm ac}^{\rm 2DEG} = \frac{G_\Box V_{\rm ac}^2}{2(\omega\tau)^2}.$$

It is easier to estimate the photon-induced current for transverse polarization. In this case, the α parameter for the pinch-off regime (so that only the first subband electron transport need be considered) is roughly

$$\alpha \approx 0.2\frac{eE_{\rm ac}d}{\hbar\omega} = 0.2\frac{eV_{\rm ac}}{\hbar\omega}\frac{d}{D},$$

where d is the channel width at the classical turning point of the second subband, which is equal to the Fermi wavelength λ_F in our approximation of infinite side walls. $\lambda_F \approx 400$ Å for a typical electron density $n_{\rm 2D} \approx 4\times10^{11}$ cm^{-2}.[3] In the low ac power limit such that $\alpha \ll 1$, only the one-photon absorption processes need to be considered, with $J_{\pm1}^2(\alpha) \approx \alpha^2$. Thus, from Eq. (28), ignoring the impedance mismatch factor,

$$\Delta I_{\rm dc} \approx \Delta V_{\rm dc}\frac{2e^2}{h}\alpha^2.$$

This gives for the current responsivity in the one-photon limit and when the device is biased near the pinch-off threshold:

$$R_I \approx 0.08\frac{d^2}{D^2}\frac{e^2\tau^2\Delta V_{\rm dc}}{\hbar^2 G_\Box}\frac{2e^2}{h}. \tag{30}$$

It should be pointed out that from Eq. (30), the current responsivity is proportional to the dc drain/source bias voltage $\Delta V_{\rm dc}$. However, $\Delta V_{\rm dc}$ should be limited to be less than the difference $[E_1(0) - E_F]/e$, which is determined by the photon voltage $\hbar\omega/e$, so that the finite bias voltage will not produce any significant dark current in the absence of radiation. Using a reasonable criterion that $\Delta V_{\rm dc} = \hbar\omega/2e$, Eq. (30) becomes

$$R_I \approx 0.04\frac{d^2}{D^2}\frac{e\tau^2\omega}{\hbar G_\Box}\frac{2e^2}{h}. \tag{31}$$

Thus, according to Eq. (31), the current responsivity of the quantum point-contact devices increases linearly with the frequency ω, while the quantum efficiency $R_Q = e/\hbar\omega$ decreases as ω^{-1}. This difference arises from the Drude model approximation which we used to calculate the ac power dissipation (in which $P_{\rm ac} \propto \omega^{-2}$). As the frequency increases, R_I will increase, corresponding to the sharp drop-off of the Drude dissipation in the 2DEG away from the point contact. It is important to note that the R_I from our consideration above does not include the dissipation associated with the quantum absorption of photons at the quantum point contact, which gives electrons excess energy of $\hbar\omega$ so that they can transmit above the potential barrier created by the point contact. Thus as R_I approaches R_Q as frequency is increased, the quantum dissipation at the point contact starts to dominate over the classical one in the bulk 2DEG. In this limit the responsivity of the device should then be replaced by just the quantum efficiency responsivity $R_Q = e/\hbar\omega$. Thus a simple rule of thumb that we propose is that as long as R_I from our formula is much smaller than R_Q, we can use it to account for the responsivity of the entire device, neglecting quantum dissipation processes associated with electron transitions at the quantum point contact. When the R_I that we calculate using Eq. (31) is comparable or even larger than R_Q, we should replace it by the quantum efficiency value $e/\hbar\omega$, i.e., R_Q is the *upper bound* of the responsivity of the device. Physically, this corresponds to the limit when energy loss from the photon field which drives the energy gaining quantum transitions of electrons dominate over that from Joule heating in the 2DEG.

It is also important to note that the current responsivity R_I in the limit $\omega\tau \gg 1$ is proportional to the square of the mobility (which is proportional to τ) of the sample. Thus samples with high electron mobilities are required for successful detector applications.

At 1 THz, for the following realistic parameters for a typical high mobility sample (with a mobility $\mu \approx 10^6$ cm^2/V s at $T \approx 1$ K), $\tau \approx 40$ ps, $G_\Box \approx 0.1\ \Omega^{-1}$, $d \approx \lambda_F \approx 400$ Å, and $D \approx 1000$ Å, we find a responsivity

$$R_I \approx 80A/W.$$

Comparing this to the quantum efficiency $R_Q = e/\hbar\omega \approx 240A/W$ at 1 THz, we find the efficiency of our device to be about $R_I/R_Q \approx 0.33$. Since the quantum efficiency decreases as ω^{-1}, we claim that the current responsivity of our quantum point-contact devices can be made to be quite close to the quantum efficiency upper bound at frequencies above 1 THz. This point makes the prospect of using quantum point-contact devices as photon detectors at THz frequency range quite appealing.

It should be pointed out, however, that the ac power $P_{\rm ac}$ used in the above calculation of the current responsivity is the power that is actually dissipated in the quantum point-contact devices. For real applications, it is the photon-induced current divided by the available ac power $P_{\rm avail}$ that determines the sensitivity of the device. Only when the ac conductance of the quantum point-contact device matches that of the planar antenna which is used to couple the radiation then the dissipated power $P_{\rm ac}$ is equal to the available power $P_{\rm avail}$. For our device, the ac conductance at 1 THz is about $G_{\rm ac} \approx G_\Box/(\omega\tau)^2 \approx 1.6\times10^{-6}\ \Omega^{-1}$. This is three-to-four orders of magnitude smaller than that of a typical antenna. Thus an impedance transformer must be used to match the impedance of the antenna R_A to that of the quantum point contact $G_{\rm ac}^{-1}$, which will result in a small fractional bandwidth of $\delta\omega/\omega \sim R_A G_{\rm ac}$.[16]

VI. DISCUSSIONS

In this section we discuss a few physical points related to the results we obtained above.

A. Photocurrent is generated near the classical turning point

We first reemphasize the key point that the most important electron transition processes which lead to siz-

able photocurrent occur near the classical turning point for each subband $x \sim -x_n^c$. In other regions electrons obey WKB approximations and propagate adiabatically without gaining longitudinal momentum which is crucial for transmission above the potential barrier. Near the classical turning point, the WKB approximation breaks down, and an analysis of the perturbed wave functions using a linearized barrier potential leads to the realization that the transition probability for absorbing m photons is roughly $J_m^2(\alpha)$, with $\alpha \approx eE_{\rm ac}x_n^c/\hbar\omega$ in the longitudinal case and $\alpha \approx eV_{\rm ac}(x_{n+1}^c)/\hbar\omega$ in the transverse case. Since α plays the role of a coupling strength to the photon field, it is crucial that one maximize the ac field strength near the classical turning points. As a practical matter, this means that one must concentrate the ac field strength as close as possible to the central region of the point contact. This should be an important consideration for any design of quantum point-contact device as photodetectors.

B. Generalization to the nonlinear regime

Our results can be readily generalized to treat the case of a large drain/source (D/S) voltage bias, following related work on point contacts without ac radiation.[17] For simplicity, and bearing in mind the potential application of the point-contact device as photodetectors, we concentrate on the pinch-off regime $d(0) < \lambda_F/2$, such that the D/S current in the absence ac radiation or large D/S voltage is negligibly small.

The effect on a large D/S voltage V can be modeled by assigning two different chemical potentials: $\mu_l = E_F + \beta eV$ for the left reservoir and $\mu_r = E_F - (1-\beta)eV$. Usually one assumes perfect left/right symmetry, such that the voltage drops on both sides of the point contact are the same, i.e., $\beta = 1/2$.

First let us review the situation in the absence of an ac field and at zero temperature. In the pinch-off regime, we have $E_F < E_1(0)$ (see Fig. 2). So we see that as the D/S voltage V is increased beyond the critical value $[E_1(0) - E_F]/\beta e$, such that $\mu_l \geq E_1(0)$, the D/S current will become

$$I_{\rm dc} = \frac{2e}{h}[\mu_l - E_1(0)], \tag{32}$$

with a differential conductance $g \equiv \frac{dI_{\rm dc}}{dV} = 2\beta e^2/h$, for $V \geq V_c = [E_1(0) - E_F]/\beta e$. Thus there is a jump for the differential conductance from 0 to $2\beta e^2/h$ at $V = V_c$. Repeating our analysis in Secs. III and IV for the present nonlinear case leads to the following result for the differential conductance in the nonlinear regime:

$$g = \frac{2\beta e^2}{h}\sum_{n=1}^{\infty}\sum_{m=-\infty}^{+\infty} f_T\{-[E_F + \beta eV m\hbar\omega - E_n(0)]\} \times J_m^2(\alpha_n^m)\left(\frac{2k_n}{k_n + k_n^m}\right)^2, \tag{33}$$

for the longitudinal polarization, and a similar expression for the transverse one. Thus for a fixed gate voltage [fixed E_F and $E_n(0)$], the effect of increasing nonlinear D/S bias is essentially the same as increasing E_F (or changing the gate voltage) in the linear regime, with ministep structures appearing before V_c is reached, at low temperatures $k_BT \ll \hbar\omega$. One also expects minipeaks in the curves of $\frac{dg}{dV} = \frac{d^2I_{\rm dc}}{dV^2}$ as a function of D/S voltage V.

C. Separating heating from photon-assisted quantum transport

An important difficulty for experimentally observing the photon-assisted quantum transport behavior discussed above is that it is often difficult to separate the effect of heating from quantum transport processes. In this aspect, our situation with the quantum point-contact device here is quite different from the photon-assisted tunneling structures in superconductor-insulator-superconductor (SIS) tunnel junctions. In SIS junctions, the superconducting energy gap in the leads prohibits energy absorptions anywhere except across the tunnel barrier, provided the frequency is below the energy gap. In a two-dimensional electron gas, however, the excitation is gapless. Therefore, photon-assisted quantum transport will always be accompanied by heating effects due to free-carrier absorptions. In the case of heating of the electron gas by the application of the ac power, the quantized conductance steps become smeared by the simple Fermi function $f_{T'}[-(E_F - E_n(0)]$, with $T' > T$, which we depict qualitatively in Fig. 3(c), whereas the photon-assisted quantum transport gives ministeps as depicted in Fig. 3(a). Therefore it is crucial to be able to minimize sample heating such that the resultant temperature $T' \ll \hbar\omega$, and to maximize the photon-assisted quantum process (by increasing the field strength near the classical turning point) so that the ministeps are more pronounced compared to the thermal smearing. Minimizing heating can be achieved, for instance, by using samples with a high electron mobility μ since the dissipation is proportional to the inverse of the square of the scattering time τ which is proportional to μ and by making the area of the two-dimensional electron gas (the mesa) small so the total dissipation is minimized. To enhance the quantum process, from the discussion at the beginning of this section, it is important to concentrate the radiation electric field into regions near the classical turning points, which is only a few hundred angstroms from the center of the point contact. Thick (approximately a few thousands angstrom) metal films with a high conductivity (preferably superconducting films) are probably the best choice for making the ac contacts/antenna.

D. Implications for detector applications

The effect of the photon-assisted quantum transport, if successfully demonstrated, can be utilized to develop novel far-infrared (or THz) detectors. THz frequencies remain one of the most underdeveloped frequency range in the electromagnetic spectrum. Present technology uses either SIS junctions or Schottky diodes for detectors. Both devices are tunnel devices, thus they have

large values of specific capacitance due to the sandwich geometry. This large junction capacitance is detrimental to high-frequency applications of both SIS and Schottky devices. In the quantum point-contact devices, however, this capacitive shunting will not be a serious problem. Because of the planar structure, the device capacitance will be much smaller than in SIS and Schottky devices. This attractive feature could make the antenna-coupled quantum point contacts quite efficient quantum photon detectors at frequencies at or above the 1-THz mark.

ACKNOWLEDGMENTS

We thank the Lorentz Institute for Theoretical Physics at the University of Leiden, where part of this work was performed, for hospitality. This work was supported in part (at UCLA) by the ONR under Grant No. N00014-90-J-1829, the Alfred P. Sloan Foundation, (at MIT) the ARO under Grant No. DAAL03-92-G-0251, and the NSF under Grant No. 9109330-ECS.

[1]B. J. van Wees, H. van Houten, C. W. J. Beenakker, J. G. Williamson, L. P. Kouwenhoven, D. van der Marel, and C. T. Foxon, Phys. Rev. Lett. **60**, 848 (1988).

[2]D. A. Wharam, T. J. Thornton, R. Newbury, M. Pepper, H. Ajmed, J. E. F. Frost, D. G. Hasko, D. C. Peacock, D. A. Ritchie, and G. A. C. Jones, J. Phys. C **21**, L209 (1988).

[3]C. W. J. Beenakker and H. van Houten, in *Solid State Physics*, edited by H. Ehrenreich and D. Turnbull (Academic, New York, 1991), Vol. 44, pp. 1–228, and references therein.

[4]Q. Hu, Appl. Phys. Lett. **62**, 837 (1993).

[5]P. K. Tien and J. P. Gordon, Phys. Rev. **129**, 647 (1963).

[6]A. H. Dayem and R. J. Martin, Phys. Rev. Lett. **8**, 246 (1962).

[7]R. A. Wyss, C. C. Eugster, and J. A. del Alamo, and Q. Hu (unpublished).

[8]D. B. Rutledge, D. P. Neikirk, and D. P. Kasilingam, in *Infrared and Millimeter Waves*, edited by K. J. Button (Academic, New York, 1983), pp. 1–90.

[9]H. C. Liu, *Superlatt. Microstruct.* **12**, 17 (1992).

[10]F. Hekking and Yu. V. Nazarov, Phys. Rev. B **44**, 11 506 (1991).

[11]Y. Imry, in *Directions in Condensed Matter Physics*, edited by G. Grinstein and G. Mazenko (World Scientific, Singapore, 1986), pp. 101–164.

[12]L. I. Glazman, G. B. Lesovik, D. E. Khmelnitskii, and R. I. Shekhter, Pis'ma Zh. Eksp. Teor. Fiz. **48**, 218 (1988) [JETP Lett. **48**, 238 (1988)].

[13]M. Buttiker and R. Landauer, Phys. Rev. Lett. **49**, 57 (1982).

[14]R. Bruinsma and P. Bak, Phys. Rev. Lett. **56**, 420 (1986).

[15]L. I. Landau and E. M. Lifshitz, *Quantum Mechanics* (Pergamon, Oxford, 1976), p. 74.

[16]D. V. Averin and K. K. Likharev, in *Single Charge Tunneling*, edited by H. Grabert and M. H. Devoret (Plenum, New York, 199), pp. 311–332.

[17]L. P. Kouwenhoven, B. J. van Wees, C. J. P. M. Harmans, J. G. Williamson, H. van Houten, C. W. J. Beenakker, C. T. Foxon, and J. J. Harris, Phys. Rev. B **39**, 8040 (1989).